Synthesis of graphene/methylene blue/ gold nanoparticles composites based on simultaneous green reduction, in situ growth and self-catalysis

Haitao Han, Dawei Pan, Xuran Wu, Qing Zhang & Haiyun Zhang

Journal of Materials Science
Full Set - Includes `Journal of Materials Science Letters'

ISSN 0022-2461
Volume 49
Number 14

J Mater Sci (2014) 49:4796-4806
DOI 10.1007/s10853-014-8179-2

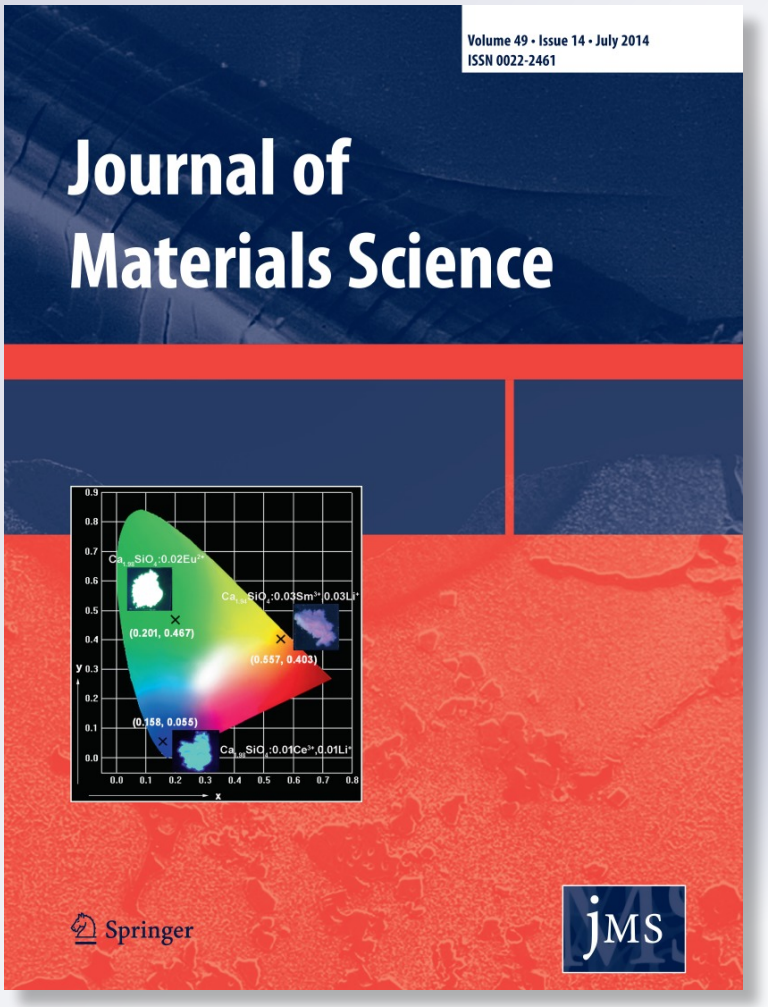

Springer

J Mater Sci (2014) 49:4796–4806
DOI 10.1007/s10853-014-8179-2

Synthesis of graphene/methylene blue/gold nanoparticles composites based on simultaneous green reduction, in situ growth and self-catalysis

Haitao Han · Dawei Pan · Xuran Wu · Qing Zhang · Haiyun Zhang

Received: 29 September 2013 / Accepted: 15 March 2014 / Published online: 1 April 2014

Abstract The novel composites based on reduced graphene oxide/methylene blue/gold nanoparticles (rGO/MB/AuNPs) were synthesized by a green and easy method. This synthesis was realized through a one-step green reduction of graphene oxide and chloroauric acid by ascorbic acid, with MB as the assistant reductant and formed AuNPs as the self-catalyst. Except for electroactive substance, MB, which was firmly coated onto the surface of rGO through π–π stacking non-covalent interactions, also serves as the anchor for AuNPs in situ growth due to the electrostatic attraction between positively charged MB and negatively charged chloroauric ions. The characteristics of rGO/MB/AuNPs composites were investigated by various optical and electrical methods. These composites exhibit excellent electrochemical properties and promising prospects for practical application in electrochemical analysis.

Introduction

Graphene (GN) is a monolayer of sp2-hybridized carbon atoms packed into a dense honeycomb crystal structure. It has attracted considerable attention from a variety of experimental and theoretical communities and has been a sought-after area of research in materials science and other subjects rapidly, since it was successfully prepared through mechanical cleavage from graphite by Geim and his co-workers [1]. Because of its unique structure, GN possesses a series of outstanding properties, such as excellent electrical and thermal conductivity [2, 3], unique optical properties [4], large specific surface area [5], excellent biocompatibility [6, 7], high mechanical strength, and good transparency [8]. These excellent properties endow GN with the tremendous potential for application in touch screens, capacitors, spintronic devices, fuel cells, batteries, sensors, transparent conductive films, high-frequency circuits, toxic material removal, and flexible electronics [9]. In the field of electrochemical sensors, GN is a beneficial material that has been extensively used as electrodes

H. Han · X. Wu (✉)
School of Chemistry and Chemical Engineering, Yantai University, Yantai 264005, People's Republic of China
e-mail: ytdxwxr@126.com

H. Han
e-mail: ytuhht@163.com

H. Han · D. Pan (✉) · Q. Zhang · H. Zhang
Key Laboratory of Coastal Zone Environmental Processes and Ecological Remediation, Yantai Institute of Coastal Zone Research (YIC), Chinese Academy of Sciences (CAS), Yantai 264003, Shandong, People's Republic of China
e-mail: dwpan@yic.ac.cn

Q. Zhang
e-mail: zhang_qing0918@163.com

H. Zhang
e-mail: hai999yun666@163.com

H. Han · D. Pan · Q. Zhang · H. Zhang
Shandong Provincial Key Laboratory of Coastal Zone Environmental Processes, YICCAS, Yantai 264003, Shandong, People's Republic of China

Q. Zhang
The Key Lab in Molecular and Nano-materials Probes of the Ministry of Education of China, College of Chemistry, Chemical Engineering and Materials Science, Shandong Normal University, Jinan 250014, People's Republic of China

modifier because of its super electrochemical properties. Electrodes modified with GN have already been used to detect β-nicotinamide adenine dinucleotide [10], glucose [11], DNA, and ethanol [12], as well as to the selective detection of dopamine (DA) [13]. Thus far, several methods have been developed to produce GN; these include mechanical cleavage, the epitaxial growth of GN on a substrate, bottom-up fabrication, and the chemical derivation of GN from graphene oxide (GO) [1, 14–17]. Despite these progresses, the method for producing single sheet GN is limited, because it involves laborious mechanical peeling of graphite layers and subsequent electrode attachment with electron beam lithography; these constraints severely limit the study and application of GN [18]. Chemical or thermal conversion from GO is the most suitable method for the low-cost and large-scale production of GN due to the easy preparation of GO from natural graphite by the modified Hummers' method [19]. GN derived from the chemical or thermal conversion of GO is also called reduced graphene oxide (rGO). Despite its wide use in various fields, GN possesses zero band gap and inertness to reaction which seriously limits its competitive strength in the field of semiconductors and sensors [9]. In other words, rGO requires decoration with other functional materials to improve its properties. To explore new properties and applications of rGO, researchers have been devoting substantial effort toward designing and constructing composites derived from rGO with superior properties. A lot of functional nanocomposites derived from rGO have been developed and applied in catalysts [8, 20, 21], sensors [12, 22], electronics and optoelectronics [23–25], and electrochemical energy storage [5, 26–28]. These functional nanomaterials could be fabricated by the functionalization of rGO on the basal plane or by the bottom-up self-assembly through direct chemical synthesis [29]. Among these methods, decoration with metal nanoparticles and chemical modification with other functional molecules are the most efficient ways to improve the properties of rGO; such techniques enhance rGO by forming a new property profile.

Over the past decades, nanoparticles, especially noble metal nanoparticles, have been widely applied to the fabrication of rGO-based functional nanomaterials. Gold nanoparticles (AuNPs) possess a series of excellent properties, such as large surface-to-volume ratio, outstanding electrical properties, high surface reaction activity, and strong adsorption ability, and these are helpful in improving rGO properties. Due to these fantastic properties, AuNPs have been extensively used as rGO decorators [19, 30, 31]. To date, most composites that combine rGO with AuNPs were synthesized through co-reduction of the precursors, chloroauric acid ($HAuCl_4$) and GO, by chemical reductants, such as sodium borohydride ($NaBH_4$) and hydrazine (N_2H_4) [32–34]. Although this method is popular, its primary disadvantage is the use of highly toxic reductants ($NaBH_4$, N_2H_4) [35]. This problem has prompted researchers to explore new and green reductants to realize the co-reduction of the precursors, instead of $NaBH_4$ or N_2H_4 [35, 36]. The use of environment-friendly ethylene glycol and ascorbic acid (AA) as green reductants for GO and noble metal precursors has been reported as an alternative method [36, 37]. AA was chosen as the main reductant in the current work. Nevertheless, AA as the single reductant cannot reduce GO adequately in an easy synthesis process. As a result, electro-conductivity would dramatically decrease under failure to the thorough reduction of GO.

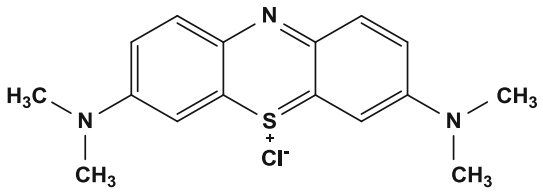

Scheme 1 MB structure

Another efficient way of fabricating rGO-based functional composites is chemically modifying rGO by using other functional molecules. Methylene blue (MB, Scheme 1) is a typical cationic organic dye full of π electrons. It is a well-established electron mediator that has been frequently used in chemical and biochemical sensors [38–42]. As reported, the π–π stacking interactions between aromatic compounds (such as MB) and rGO essentially lead to a stable adsorption of aromatic compounds onto the surface of rGO. The MB adsorbed on the surface of rGO enables it to bear a positive charge, avoiding the aggregation of rGO and increasing its dispersity [43]. Furthermore, positively charged MB on the rGO surface can attract $AuCl_4^-$ through the electrostatic attraction, and this MB serves as the anchor for AuNPs in situ growth.

In this study, novel rGO/MB/AuNPs composites were synthesized through a green and easy method, in which GO and $HAuCl_4$ were subjected to simultaneous green reduction using AA as the main and MB the auxiliary reductant and the formed AuNPs as the self-catalyst. MB served as the anchor for AuNPs in situ growth given the electrostatic attraction between MB and $AuCl_4^-$. The adsorption of MB onto rGO prevents the aggregation of the composites, thereby increasing their dispersity. The composites were characterized by various optical and electrical methods, including X-ray photoelectron spectroscopy (XPS), X-ray diffraction spectroscopy (XRD), scanning electron microscopy (SEM), transmission electron microscopy (TEM), cyclic voltammetry (CV), and so on. Each component of the

proposed composites plays its unique role in the synthesis process. Essentially, AA was the main reductant. MB was the assistant reductant and electroactive substance, as well as the anchor for AuNPs in situ growth. AuNPs can facilitate electron transfer and as the self-catalyst to catalyze the reduction of GO by AA. The composites exhibit an excellent response to the oxidation of uric acid (UA), DA, and AA. They also present promising prospects for practical application in electrochemical analysis.

Experimental

Reagents and apparatus

GO (1 to 5 μm diameter, 0.8 to 1.2 nm thickness, and greater than 99 % purity) was purchased from Nanjing JCNano technology Co., Ltd., China. MB, $HAuCl_4$, and AA were supplied by Sinopharm Chemical Reagent Co., Ltd. All other chemicals are analytical reagents used without further purification. Deionized water (18.2 MΩ cm specific resistance) obtained from Pall Cascada laboratory water system was used throughout.

SEM images were taken with a Hitachi S-4800 microscope (Japan), and TEM images were obtained on JEM-1400/S TEM system (JEOL). Energy dispersive X-ray spectroscopy (EDS) was obtained using a HORIBA EX-350 energy dispersive spectrometer (Japan). XPS measurements were carried out on a Kratos Amicus spectrometer. XRD was performed using an X-ray diffractometer (XRD-7000, Shimadzu Corporation). Fourier transformation infrared (FTIR) spectra were recorded with a Nicolet iS 10 infrared spectrometer. UV–Vis spectra were obtained using a DU 800 ultraviolet and visible spectrophotometer. All the electrochemical experiments were performed on a CHI 660D Electrochemical Work Station. A conventional three-electrode system consisting of a modified glassy carbon (GC) working electrode, a platinum foil auxiliary electrode, and a silver chloride (Ag/AgCl) reference electrode was employed. All the potentials in this paper were considered with respect to the Ag/AgCl reference electrode.

Synthesis of rGO/MB/AuNPs composites

GO (20 mg) was dispersed in 30 mL deionized water with ultrasonication for 1 h. After 4 mL MB (1 mmol L^{-1}) was added to the suspension, the mixture was stirred for 10 min. Then, 0.5 mL $HAuCl_4$ (20 mmol L^{-1}) was added and stirred for another 10 min. Finally, 2 mL AA (100 mmol L^{-1}) was added, and the mixture was kept at 100 °C for 1 h with magnetic stirring. The mixed suspension was filtered and thoroughly washed with deionized water. At last, the target rGO/MB/AuNPs composites were obtained after the residues were dried in a vacuum drying chamber. Similar procedures were used to prepare rGO and rGO/MB composites. ICP-MS measurement exhibits the content ratio of Au in the rGO/MB/AuNPs composites is 7.2 % (8.5 % theoretically).

Fabrication of rGO/MB/AuNPs composites modified electrode

rGO/MB/AuNPs powder (2.5 mg) was dispersed in 5 mL ethanol to obtain the suspension (0.5 mg mL^{-1}). The rGO/MB/AuNPs powder easily dispersed in ethanol with ultrasonication for 10 min. Before use, the GC electrode was mechanically polished over a microcloth with 0.05-μm alumina slurry, rinsed, and then ultrasonicated with deionized water. rGO/MB/AuNPs suspensions (3 μL) were dropped on the surface of GC electrode and dried with an infrared lamp to obtain the rGO/MB/AuNPs composites modified GC (rGO/MB/AuNPs/GC) electrode. Similarly, rGO modified GC (rGO/GC) and rGO/MB composites modified GC (rGO/MB/GC) electrodes were prepared.

Electrochemical procedure

The rGO/MB/AuNPs composites were electrochemically characterized by CV and differential pulse voltammetry (DPV) techniques. The rGO/MB/AuNPs/GC electrode was placed in a voltammetric cell with 10 ml electrolyte solution during the electrochemical measurements. The CV experiments were carried out in 0.5 mol L^{-1} sulfuric acid (H_2SO_4) solution at the potential range of −0.2 to 1.0 V and the scan rate of 100 mV s^{-1}. The bare GC, rGO/GC, and rGO/MB/GC electrodes were treated under the same conditions. The response of rGO/MB/AuNPs/GC electrode to the oxidation of UA, DA, and AA was investigated by DPV (from −0.6 to 0.8 V) in phosphate buffer solution (PBS, pH 7.4).

Results and discussion

To investigate their structure and properties, the rGO/MB/AuNPs composites were characterized by Fourier transformation infrared spectroscopy (FTIR), UV–Vis spectroscopy (UV–Vis), XPS, XRD, SEM, TEM, and electrochemical methods. The potential application of rGO/MB/AuNPs composites in electrochemical analysis was also investigated by the DPV techniques.

FTIR spectrum of the rGO/MB/AuNPs composites

FTIR spectroscopy was conducted to investigate the reduction and functionalization of GO during the synthesis

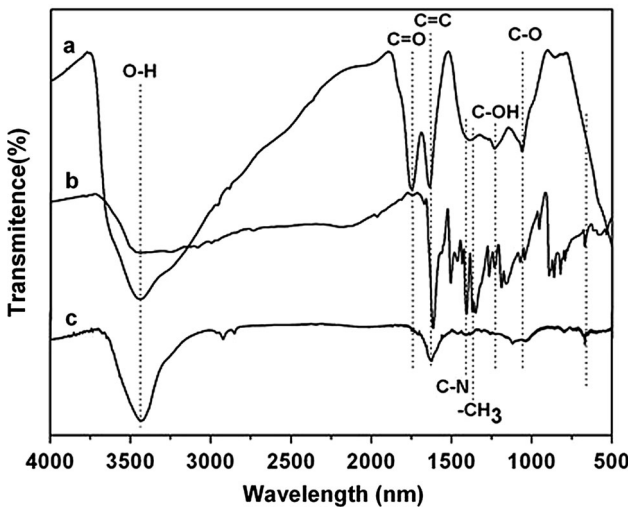

Fig. 1 FTIR spectra of GO (*a*), MB (*b*), and rGO/MB/AuNPs composites (*c*)

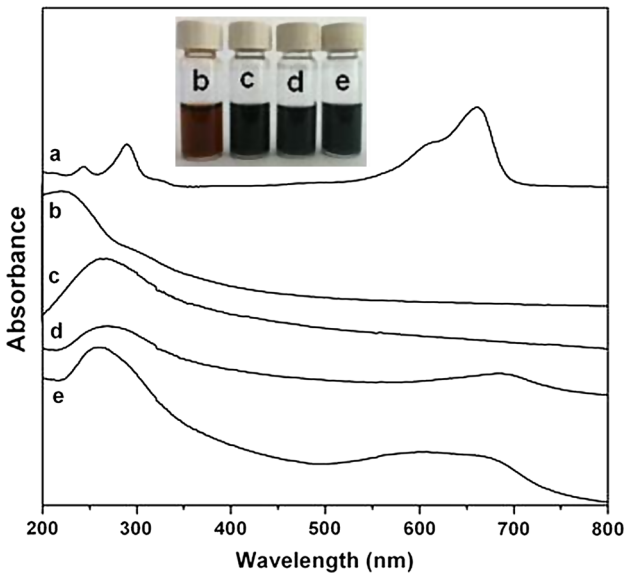

Fig. 2 UV–Vis spectra of MB (*a*), GO (*b*), rGO (*c*), rGO/MB (*d*), and rGO/MB/AuNPs composites (*e*). *Inset*: corresponding digital photographs

process (Fig. 1). The FTIR spectrum of GO (Fig. 1a) shows the broad peak at 3398 cm^{-1} which is assigned to the O–H stretching vibration. The other characteristic absorption peaks at 1727, 1219, and 1052 cm^{-1} which correspond to the stretching of C=O (carbonyl), C–OH, and C–O (alkoxy) bonds, respectively, are also observed [35, 44]. All these peaks serve as the evidence for the existence of oxygen-containing groups on GO. The FTIR spectrum of MB (Fig. 1b) exhibits its typical symmetric C–N stretch at 1398 cm^{-1}, symmetric $–CH_3$ deformation at 1354 cm^{-1}, and absorption peak at 661 cm^{-1} [41]. As to the FTIR spectrum of rGO/MB/AuNPs composites (Fig. 1c), the characteristic absorption peaks of oxygen-containing groups at 1727 cm^{-1} (ν C = O), 1219 cm^{-1} (ν C–OH) almost disappear, and the peak at 1052 cm^{-1} (ν C–O) significantly decreases, indicating that GO is reduced to rGO. Moreover, all the characteristic absorption peaks of MB can be observed on the FTIR spectrum of the rGO/MB/AuNPs composites. These results indicate that GO can be reduced to rGO and be coated with MB onto its surface with this proposed method.

UV–Vis spectrum of the rGO/MB/AuNPs composites

Figure 2 shows the UV–Vis spectrum of the rGO/MB/AuNPs composites. Figure 2a shows that MB has its own typical UV–Vis absorbance at 660 nm. Figure 2b shows the UV–Vis spectrum of GO with its typical absorbance peak at 223 nm which is similar to the reported values [32]. Compared to GO, the absorbance peak of rGO shifts to about 261 nm (Fig. 2c), indicating that GO can be reduced to rGO [19]. As to rGO/MB (Fig. 2d), a new peak appears at about 675 nm, indicating the coating of MB onto the rGO surface. Figure 2e shows the UV–Vis spectrum of rGO/MB/AuNPs composites, which includes all the absorbance peaks of rGO/MB. However, when compared with rGO/MB, the rGO/MB/AuNPs exhibit a broad peak between 500 and 600 nm; this result can be explained the existence of AuNPs. The inset in Fig. 2 is the digital images of GO (b), rGO (c), rGO/MB (d), and rGO/MB/AuNPs (e) dispersion. Compared with the brown color GO, the three other samples are black which is the color of rGO, further confirming that GO can be reduced to rGO under the proposed scheme. All the above-mentioned phenomena suggest the successful synthesis of the rGO/MB/AuNPs composites.

SEM images and EDS pattern of the rGO/MB/AuNPs composites

To describe the morphology of the as-synthesized rGO/MB/AuNPs composites, SEM was employed. Figure 3 illustrates the typical SEM photographs of rGO (Fig. 3a), rGO/MB (Fig. 3b), and rGO/MB/AuNPs (Fig. 3c), as well as the EDS pattern of the rGO/MB/AuNPs composites (Fig. 3d). Figure 3a shows large flakes of rGO with slightly scrolled edges form. Due to their partial aggregation, rGO flakes fold together. However, the morphology of rGO/MB shows significant differences. The morphology of rGO/MB is more fragmentized considerably rougher than that of rGO. This result can be attributed to the adsorption of MB onto the rGO surface. The morphology of rGO/MB/AuNPs is similar to that of rGO/MB, except for the uniformly distributed AuNPs on the surface of composites. The EDS pattern (Fig. 3d) indicates that C, O, F, Na, Al, Au, and Cl

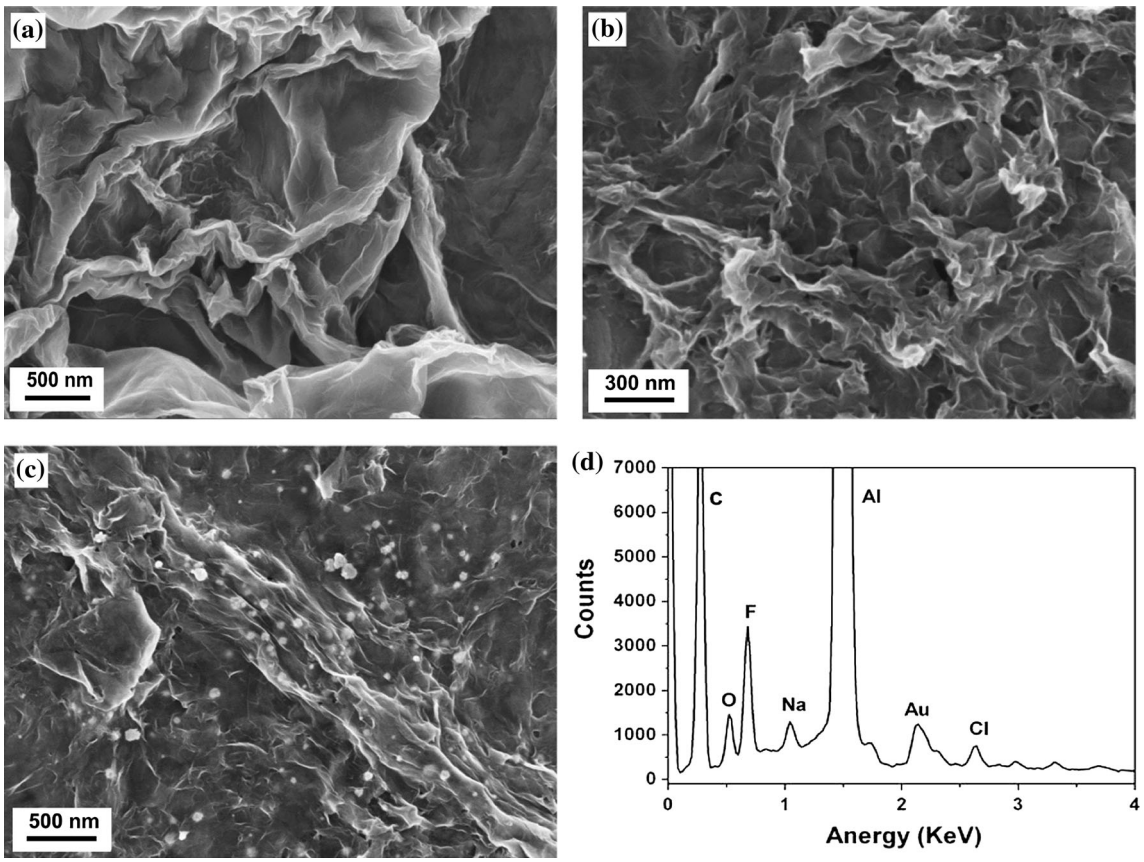

Fig. 3 SEM images of rGO (**a**), rGO/MB (**b**), rGO/MB/AuNPs composites (**c**), and EDS pattern of rGO/MB/AuNPs composites (**d**)

are the major elements in the rGO/MB/AuNPs composites. C, O, and Cl may come from rGO and MB, while Al, Na, and F may be attributed to base aluminum foil. The presence of Au in the pattern indicates the existence of AuNPs. Distinctly, MB molecules and AuNPs are attached onto the rGO surface.

TEM images of the rGO/MB/AuNPs composites

The TEM images provide further evidence for the successful attachment of MB and AuNPs onto rGO. Figure 4 shows the TEM photographs of rGO, rGO/MB, and rGO/MB/AuNPs composites. Figure 4a illustrates that the surface of the pure rGO is corrugated and partially curly, and that its transparency is very high. However, the surface of rGO/MB (Fig. 4b) is considerably rougher. It looks like that there is a thin membrane-like substance forms on the surface of rGO. This is caused by the coating of MB onto the rGO surface. The morphology of the rGO/MB/AuNPs (Fig. 4c) is also highly similar to that of rGO/MB—a finding that corresponds to that of SEM. Furthermore, numerous uniform nanoparticles can be observed on the surface of rGO/MB/AuNPs composites. Figure 4d shows the high magnification TEM image of the as-prepared rGO/MB/AuNPs composites. Most of the AuNPs have a diameter within 30–60 nm. The TEM results suggest the successful synthesis of the rGO/MB/AuNPs composites.

XPS spectrum of the rGO/MB/AuNPs composites

To further confirm the immobilization of MB and AuNPs into the composites and investigate the unique role of each component, XPS was conducted. Figure 5a, b, and c presents the N 1s, S 2p, and Au 4f XPS spectra of rGO/MB/AuNPs composites, respectively. The appearance of the N, S, and Au peaks in rGO/MB/AuNPs composites can be regarded as the powerful evidence for the successful synthesis of target rGO/MB/AuNPs composites. The XPS spectrum of the rGO/MB/AuNPs composites (Fig. 5c) displays a doublet for Au due to Au 4f7/2 and Au 4f5/2 spin–orbit coupling. The positions of the most important pair of peaks (BEs of 83.9 and 87.6 eV) are related to Au^0 [19]. However, the other pairs (BEs of 85.6 and 88.9 eV) are related to the Au^{+1} which is the stable gold oxide state [45]. The existence of Au^{+1} may be caused by the inadequate reduction of $HAuCl_4$. On the basis of relative peak areas, the respective atomic percentages were estimated as 89.4 % for Au^0, and 8.1 % for Au^{+1}. And these results

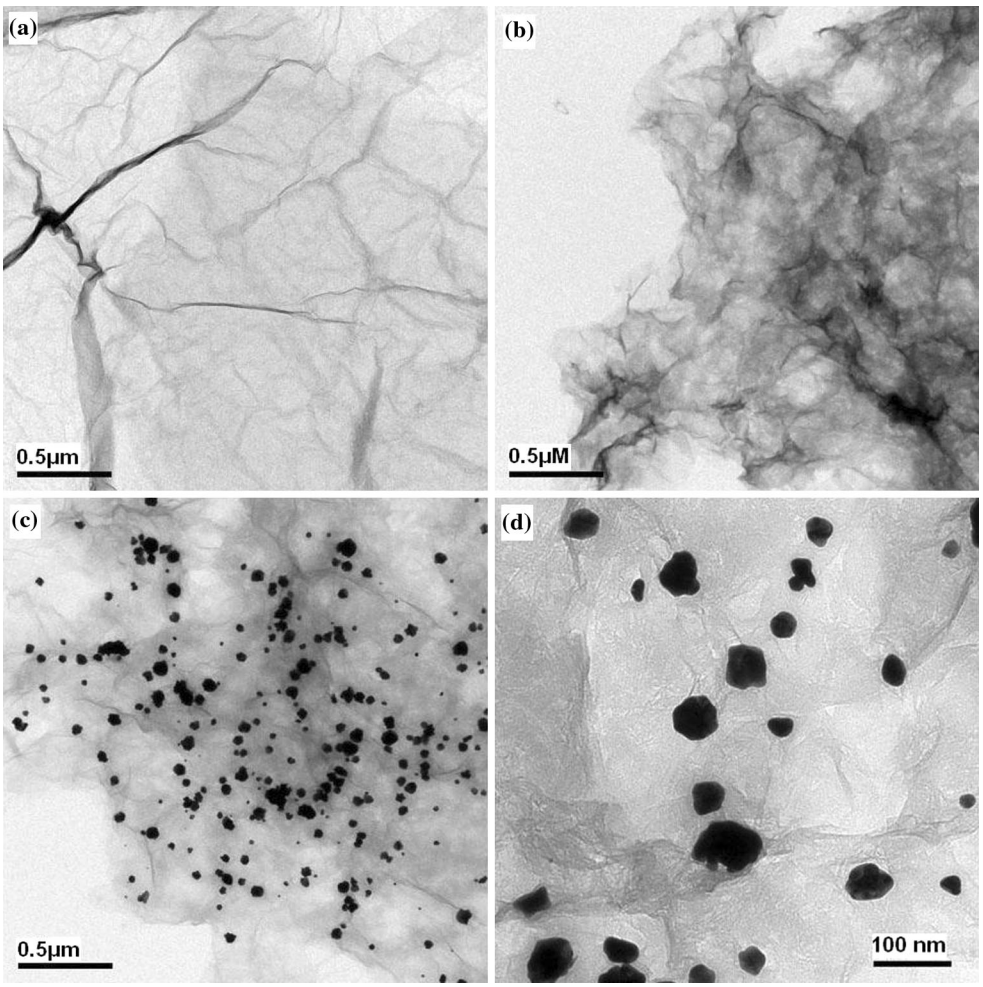

Fig. 4 TEM images of rGO (**a**), rGO/MB (**b**), and rGO/MB/AuNPs composites (**c**, **d**)

indicate that the gold atoms in the clusters are present largely as Au^0. These results correspond with the EDS pattern exhibited in Fig. 3 and can be the powerful evidence for the existence of AuNPs. The degree of GO reduction significantly influences its electro-conductivity. According to the literature [11], the degree of GO reduction can be characterized by the C/O ratio of GO-based composites. Figure 5d shows the C 1s and O 1s XPS spectra of the GO, rGO, rGO/MB, and rGO/MB/AuNPs composites. C 1s and O 1s peaks with different C/O ratios are present in all the samples. The C/O ratios of GO, rGO, rGO/MB, and rGO/MB/AuNPs composites are 64/34, 57/24, 70/22, and 80/18, respectively. When GO is reduced to rGO, the C/O ratio increases from 64/34 to 57/24, indicating the partial reduction of GO by AA in the proposed scheme. As can be seen, the C/O ratio of rGO/MB is substantially larger than that of rGO. The change may be attributed to the auxiliary reduction of MB given its reducibility. However, the C/O ratio of the rGO/MB/AuNPs composites is the largest among the four samples implying the most excellent electro-conductivity. The catalysis of AuNPs to the reduction of GO adequately explains this phenomenon [36].

XRD pattern of the rGO/MB/AuNPs composites

XRD is a powerful and effective method for the investigation of the interlayer changes and crystalline properties of as-synthesized carbon material. Figure 6 shows the XRD patterns of GO (Fig. 6a), rGO (Fig. 6b), rGO/MB (Fig. 6c), and rGO/MB/AuNPs composites (Fig. 6d). The distance between two layers of rGO is an important parameter that provides structural information of functional rGO materials [46]. As can be seen from Fig. 6a, GO exhibits a feature diffraction peak at about $2\theta = 10.9°$ (001) which is similar to the reported values [46, 47]. According to Prague formula, the interlayer d-spacing of GO is calculates as 0.81 nm. It is because of the presence and interaction of oxygen-containing functional groups on the surface of GO, can it has a so large interlayer d-spacing

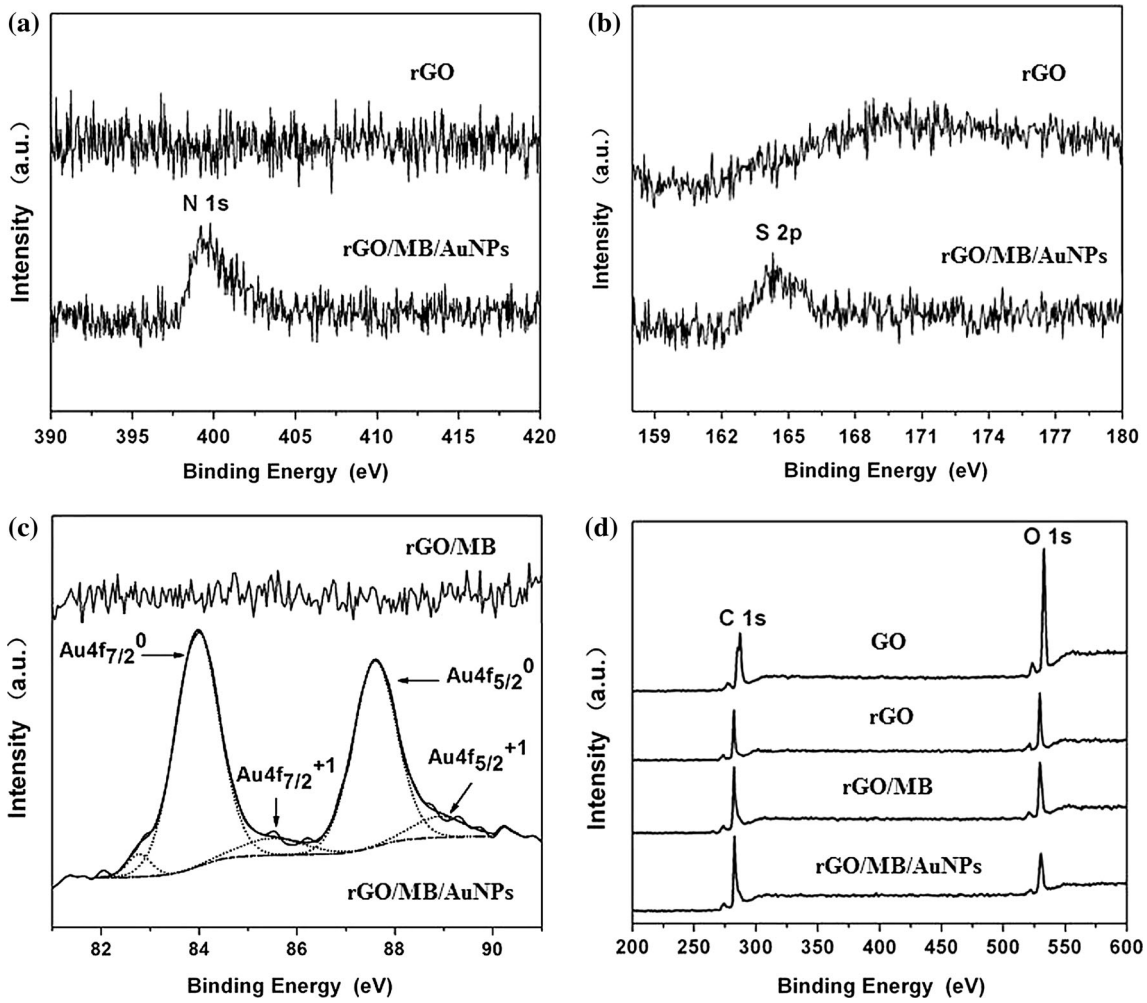

Fig. 5 N 1s (**a**), S 2p (**b**) XPS spectra of rGO and rGO/MB/AuNPs composites, Au 4f (**c**) XPS of rGO/MB and rGO/MB/AuNPs composites, and C 1s, O 1s XPS spectra of GO, rGO, rGO/MB, and rGO/MB/AuNPs composites (**d**)

and fluffy morphology with low density [46, 47]. As to the XRD pattern of rGO, the (001) peak of GO decreases partially, while there appears a small GN feature diffraction peak (002) at about $2\theta = 22.7°$ corresponding to an interlayer d-spacing of 0.39 nm. The decreases in interlayer d-spacing and (001) peak of GO may be caused by the partial removal of oxygen-containing functional groups on the GO surface during the reduction process by AA. However, when compared to GN (002) peak, the GO (001) peak is also very large which indicates that GO can be only partly reduced by AA in this experimental condition. Figure 6c shows the XRD pattern of rGO/MB, which has a much larger GN feature diffraction peak (002) and a very small (001) peak of GO. At the same time, rGO/MB has an even smaller interlayer d-spacing of 0.34 nm ($2\theta = 26.0°$) than rGO. The significant decrease of GO (001) peak and conspicuous augment of GN (001) peak with a smaller interlayer d-spacing may be attributed to the assistant reduction effect of MB. At last, the (001) peak of GO in the rGO/MB/AuNPs composites almost completely disappears, which can be explained by the catalysis of AuNPs to the reduction of GO. Furthermore, the typical diffraction peaks at $2\theta = 38.13°$, 44.21°, 64.64°, 77.60°, and 81.73° corresponding to the (111), (200), (220), (311), and (222) lattice planes of the gold face-centered cubic crystal appear attractively [48, 49]. When compared to rGO/MB, although the interlayer d-spacing of the rGO/MB/AuNPs composites should be decreased continually according to the discussion above due to the catalysis of AuNPs, it increases to 0.36 nm ($2\theta = 24.7°$). This may caused by the insertion of AuNPs into the interlayer of rGO which competes with the catalysis of AuNPs. Obviously, the effect of the insertion of AuNPs dominates the competition.

All the aforementioned results indicate that the target rGO/MB/AuNPs composites have been successfully fabricated, and that each component in the combination plays its

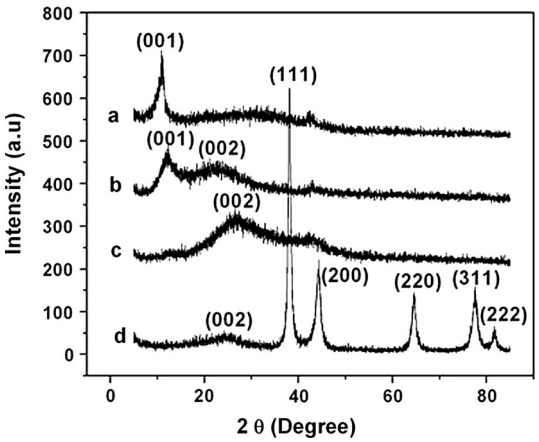

Fig. 6 XRD patterns of GO (*a*), rGO (*b*), rGO/MB (*c*), and rGO/MB/AuNPs composites (*d*)

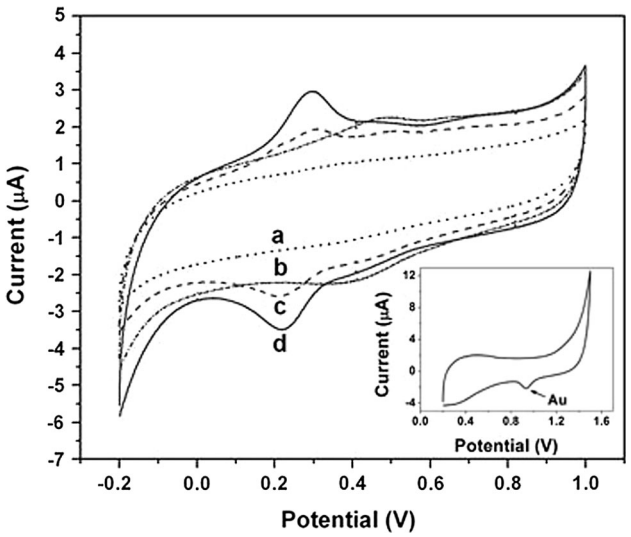

Fig. 7 Cyclic voltammograms of bare (*a*), rGO (*b*), rGO/MB (*c*), and rGO/MB/AuNPs (*d*) modified GC electrodes in 0.5 mol L^{-1} H_2SO_4 solution (scan rate 100 mV s^{-1})

unique role in the synthesis process. AA plays as the major component in the reduction of GO and $AuCl_4^-$, while rGO adsorbs MB and supports AuNPs. MB serves as the electro-active substance, the anchor for AuNPs growth, and the auxiliary reductant. AuNPs act as the self-catalyst that facilitates the reduction of GO by AA and MB. Because of the presence of MB and formed AuNPs, GO can be reduced more thoroughly in the proposed synthesis process.

Electrochemical behaviors of the rGO/MB/AuNPs composites

To investigate the electrochemical properties of the target rGO/MB/AuNPs composites, the CV curves of the bare GC, rGO/GC, rGO/MB/GC, and rGO/MB/AuNPs/GC electrodes in 0.5 mol L^{-1} H_2SO_4 solution from −0.2 to 1.0 V with a scan rate of 100 mV s^{-1} are presented in Fig. 7. As expected, no any redox peak can be observed in the CV of the bare GC electrode (Fig. 7a) within the scan range. A pair of redox peak appears at the potential range of 0.4–0.5 V for the rGO/GC electrode which may be caused by the remaining oxygen-containing functional groups on rGO surface (Fig. 7b). When compared to rGO/GC electrode, the CV of the rGO/MB/GC electrode (Fig. 7c) indicates another pair of redox peak appearing at about 0.22 V. Obviously, this pair of peak corresponds to the electro-active MB. At last, the CV curve of the rGO/MB/AuNPs/GC electrode (Fig. 7d) exhibits a considerably larger redox peak of MB. Given the facilitation of AuNPs to electron transfer, this phenomenon can be easily understood. The inset in Fig. 7 is the CV curve of rGO/MB/AuNPs modified electrode in 0.5 mol L^{-1} H_2SO_4 solution from 0.2 to 1.5 V which exhibits the peak of Au clearly. It should be noted that MB can be oxidized when the potential is larger than 1.2 V with the disappearance of the MB redox peak. The electrode modified with the proposed rGO/MB/AuNPs composites exhibits a promising prospect for practical application due to its excellent electrochemical properties.

Potential application of the rGO/MB/AuNPs composites in electrochemical analysis

AA, DA, and UA are electro-active compounds with similar electrochemical properties and almost the same oxidation peak potential [33, 50]. Due to these similarities, the electrochemical identification of these three compounds is very difficult. In this work, DPV was employed to explore the application of the target rGO/MB/AuNPs composites in electrochemical analysis. The DPV measurements were carried out in PBS (pH = 7.4) from −0.6 to 0.8 V (amplitude 0.05 V, pulse width 0.5 s) for the rGO/MB/AuNPs/GC electrode. The results are shown in Fig. 8. It can be seen that, there is only one oxidation peak of MB can be observed at about −0.3 V in PBS solution without analytes (Fig. 8a) [12, 42, 44]. With the addition of 500 μmol L^{-1} AA, there appears its oxidation peak at about 0 V (Fig. 8b) [33]. Sequentially, after the addition of 1 μmol L^{-1} DA, the oxidation peak of DA appears at about 0.17 V. Obviously, this peak does not affect the peaks of AA and MB (Fig. 8c) [33, 50]. When the solution contains 500 μmol L^{-1} AA, 1 μmol L^{-1} DA, and 10 μmol L^{-1} UA, four oxidation peaks can be observed, one of which is the UA oxidation peak at about 0.31 V (Fig. 8d) [33, 50, 51]. The inset in Fig. 8 is the curve of Fig. 8d after background substraction. These three analytes can be thoroughly separated under this proposed rGO/MB/AuNPs/GC

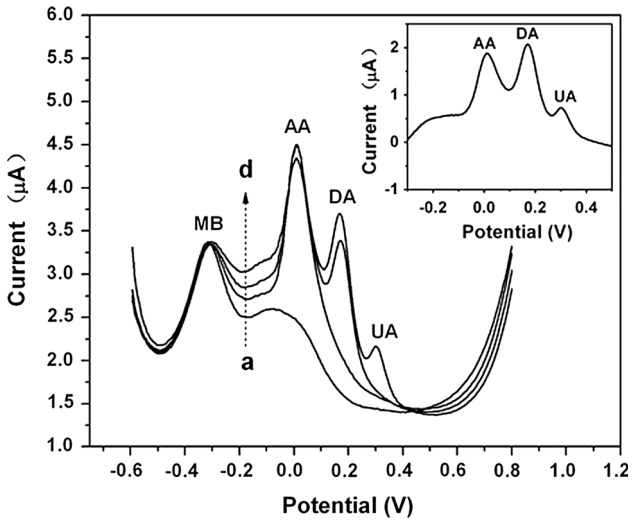

Fig. 8 Differential pulse voltammograms of rGO/MB/AuNPs/GC electrode in PBS (pH = 7.4) solution (*a*), a +500 μmol L^{-1} AA (*b*), *b* + 1 μmol L^{-1} DA (*c*), and *c* + 10 μmol L^{-1} UA (*d*). Amplitude: 0.05 V, pulse width: 0.5s. *Inset*: voltammogram of *d* after background substraction

electrode. That is, in the simultaneous detection of the three aforementioned analytes by DPV, the potential differences among the three oxidation peaks are 170 mV (AA–DA), 132 mV (DA–UA), and 302 mV (AA and UA) separately. These values are superior to those previously reported for modified electrodes [52, 53]. Preliminary experiments were carried out to explore the application of the rGO/MB/AuNPs composites modified electrode for the determination of AA, DA, and UA. Compared with previously reported nano-structured materials modified electrodes [54–57], the rGO/MB/AuNPs composites modified electrode presents a lower detection limit (2.5, 0.15, and 0.25 μmol L^{-1} for AA, DA, and UA, respectively) because of the excellent electrochemical properties of this proposed rGO/MB/AuNPs composites.

Stability of the rGO/MB/AuNPs composites was investigated by measuring the current responses to AA every few days with the rGO/MB/AuNPs composites modified electrode stored in air. After being stored for 30 days in air, the response current of the rGO/MB/AuNPs/GC electrode to AA remains 75.28 % of the initial values. To confirm whether AA would further destroy the structure of the rGO/MB/AuNPs composites during the electro-catalytic process, 40 measurements of the current responses to 0.05 mmol L^{-1} AA were done using one rGO/MB/AuNPs/GC electrode, and the RSD is only 2.6 %. In other words, AA will not further destroy the structure of the rGO/MB/AuNPs composites when AA as a substrate in the electrochemical analysis.

The rGO/MB/AuNPs composites present promising prospects for practical application in electrochemical analysis.

Conclusions

The novel rGO/MB/AuNPs composites were synthesized by a green and easy method based on the simultaneous reduction of GO and $HAuCl_4$ by AA, with MB as the auxiliary reductant and formed AuNPs as the self-catalyst. MB is firmly coated onto the rGO surface through π–π stacking non-covalent interactions and serves as the anchor for AuNPs in situ because of the electrostatic attraction between positively charged MB and negatively charged $AuCl_4^-$. Because of the novel structure and the combination of excellent properties of MB, rGO, and AuNPs, the target rGO/MB/AuNPs composites are promising materials for practical application in electrochemical analysis.

Acknowledgements This study was financially supported by the National Natural Science Foundation of China (21007087, 41276093), the Natural Science Foundation of Shandong Province (BS2010HZ030), the Taishan Scholar Program of Shandong Province, and the Youth Innovation Promotion Association of CAS.

References

1. Novoselov KS, Geim AK, Morozov SV, Jiang D, Zhang Y, Dubonos SV, Grigorieva IV, Firsov AA (2004) Electric field effect in atomically thin carbon films. Science 306:666–669
2. Bunch JS, Verbridge SS, Alden JS, van der Zande AM, Parpia JM, Craighead HG, McEuen PL (2008) Impermeable atomic membranes from graphene sheets. Nano Lett 8:2458–2462
3. Lee C, Wei XD, Kysar JW, Hone J (2008) Measurement of the elastic properties and intrinsic strength of monolayer graphene. Science 321:385–388
4. Nair RR, Blake P, Grigorenko AN, Novoselov KS, Booth TJ, Stauber T, Peres NMR, Geim AK (2008) Fine structure constant defines visual transparency of graphene. Science 320:1308
5. Stoller MD, Park SJ, Zhu YW, An JH, Ruoff RS (2008) Graphene-based ultracapacitors. Nano Lett 8:3498–3502
6. Mohanty N, Berry V (2008) Graphene-based single-bacterium resolution biodevice and DNA transistor: interfacing graphene gerivatives with nanoscale and microscale biocomponents. Nano Lett 8:4469–4476
7. Wu P, Shao Q, Hu Y, Jin J, Yin Y, Zhang H, Cai C (2010) Direct electrochemistry of glucose oxidase assembled on graphene and application to glucose detection. Electrochim Acta 55:8606–8614
8. Zhu C, Dong S (2013) Recent progress in graphene-based nanomaterials as advanced electrocatalysts towards oxygen reduction reaction. Nanoscale 5:1753–1767
9. Georgakilas V, Otyepka M, Bourlinos AB, Chandra V, Kim N, Kemp CK, Hobza P, Zboril R, Kim KS (2012) Functionalization of graphene: covalent and non-covalent approaches, derivatives and applications. Chem Rev 112:6156–6214
10. Tang L, Wang Y, Li Y, Feng H, Lu J, Li J (2009) Preparation, structure, and electrochemical properties of reduced graphene sheet films. Adv Funct Mater 19:2782–2789
11. Shan C, Yang H, Song J, Han D, Ivaska A, Niu L (2009) Direct electrochemistry of glucose oxidase and biosensing for glucose based on graphene. Anal Chem 81:2378–2382
12. Zhou M, Zhai Y, Dong S (2009) Electrochemical sensing and biosensing platform based on chemically reduced graphene oxide. Anal Chem 81:5603–5613

13. Wang Y, Li Y, Tang L, Lu J, Li J (2009) Application of graphene-modified electrode for selective detection of dopamine. Electrochem Commun 11:889–892
14. Kim KS, Zhao Y, Jang H, Lee SY, Kim JM, Kim KS, Ahn JH, Kim P, Choi JY, Hong BH (2009) Large-scale pattern growth of graphene films for stretchable transparent electrodes. Nature 457:706–710
15. Li X, Cai W, An J, Kim S, Nah J, Yang D, Piner R, Velamakanni A, Jung I, Tutuc E, Banerjee SK, Colombo L, Ruoff RS (2009) Large-area synthesis of high-quality and uniform graphene films on copper foils. Science 324:1312–1314
16. Berger C, Song Z, Li X, Wu X, Brown N, Naud C, Mayou D, Li T, Hass J, Marchenkov AN, Conrad EH, First PN, de Heer WA (2006) Electronic confinement and coherence in patterned epitaxial graphene. Science 312:1191–1196
17. Wang H, Wang X, Li X, Dai H (2009) Chemical self-assembly of graphene sheets. Nano Res 2:336–342
18. Liu X, Xie L, Li H (2012) Electrochemical biosensor based on reduced graphene oxide and Au nanoparticles entrapped in chitosan/silica sol–gel hybrid membranes for determination of dopamine and uric acid. J Electroanal Chem 682:158–163
19. Zhang Z, Chen H, Xing C, Guo M, Xu F, Wang X, Gruber H, Zhang B, Tang J (2011) Sodium citrate: a universal reducing agent for reduction/decoration of graphene oxide with au nanoparticles. Nano Res 4:599–611
20. Zhang H, Lv X, Li Y, Wang Y, Li J (2009) P25-graphene composite as a high performance photocatalyst. ACS Nano 4:380–386
21. Zhu C, Wang P, Wang L, Han L, Dong S (2011) Facile synthesis of two-dimensional graphene/SnO2/Pt ternary hybrid nanomaterials and their catalytic properties. Nanoscale 3:4376–4382
22. Zhu C, Guo S, Fang Y, Dong S (2010) Reducing sugar: new functional molecules for the green synthesis of graphene nanosheets. ACS Nano 4:2429–2437
23. Stankovich S, Dikin DA, Dommmett GHB, Kohlhaas KM, Zimney EJ, Stach EA, Piner RD, Nguyen ST, Ruoff RS (2006) Graphene-based composite materials. Nature 442:282–286
24. Wang P, Jiang T, Zhu C, Zhai Y, Wang D, Dong S (2010) One-step, solvothermal synthesis of graphene–CdS and graphene–ZnS quantum dot nanocomposites and their interesting photovoltaic properties. Nano Res 3:794–799
25. Britnell L, Gorbachev RV, Jalil R, Belle BD, Schedin F, Mishchenko A, Georgiou T, Katsnelson MI, Eaves L, Morozov SV, Peres NM, Leist J, Geim AK, Novoselov KS, Ponomarenko LA (2012) Field-effect tunneling transistor based on vertical graphene heterostructures. Science 335:947–950
26. Paek SM, Yoo E, Honma I (2009) Enhanced cyclic performance and lithium storage capacity of SnO2/graphene nanoporous electrodes with three-dimensionally delaminated flexible structure. Nano Lett 9:72–75
27. Zhu X, Zhu Y, Murali S, Stollers MD, Ruoff RS (2011) Nanostructured reduced graphene oxide/Fe2O3 composite as a high-performance anode material for lithium ion batteries. ACS Nano 5:3333–3338
28. Zhu Y, Murali S, Stoller MD, Ganesh KJ, Cai W, Ferreira PJ, Pirkle A, Wallace RM, Cychosz KA, Thommes M, Su D, Stach EA, Ruof RS (2011) Carbon-based supercapacitors produced by activation of graphene. Science 332:1537–1541
29. Tang Q, Zhou Z, Chen Z (2013) Graphene-related nanomaterials: tuning properties by functionalization. Nanoscale 5:4541–4583
30. Li S, Shi Y, Liu L, Song L, Pang H, Du J (2012) Electrostatic self-assembly for preparation of sulfonated graphene/gold nanoparticle hybrids and their application for hydrogen peroxide sensing. Electrochim Acta 85:628–635
31. Basavaraja C, Kim WJ, Thinh PX, Huh DS (2012) Electrical and magnetic properties of polyaniline-2-naphthalene sulfonic acid/gold nanoparticle-reduced graphite oxide composites. Mater Lett 77:41–44
32. Shan C, Yang H, Han D, Zhang Q, Ivaska A, Niu L (2010) Graphene/AuNPs/chitosan nanocomposites film for glucose biosensing. Biosens Bioelectron 25:1070–1074
33. Li F, Chai J, Yang H, Han D, Niu L (2010) Synthesis of Pt/ionic liquid/graphene nanocomposite and its simultaneous determination of ascorbic acid and dopamine. Talanta 81:1063–1068
34. Liu A, Huang S (2012) A glucose biosensor based on direct electrochemistry of glucose oxidase immobilized onto platinum nanoparticles modified graphene electrode. Sci China Phys Mech 55:1163–1167
35. Liu S, Wang J, Zeng J, Ou J, Li Z, Liu X, Yang S (2010) "Green" electrochemical synthesis of Pt/graphene sheet nanocomposite film and its electrocatalytic property. J Power Sources 195:4628–4633
36. Xu C, Wang X, Zhu J (2008) Graphene–metal particle nanocomposites. J Phys Chem C 112:19841–19845
37. Kim SH, Jeong GH, Choi D, Yoon S, Jeon HB, Lee SM, Kim SW (2013) Synthesis of noble metal/graphene nanocomposites without surfactants by one-step reduction of metal salt and graphene oxide. J Colloid Interface Sci 389:85–90
38. Zhang Y, Liu L, Xi F, Wu T, Lin X (2010) A simple layer-by-layer assembly strategy for a reagentless biosensor based on a nanocomposite of methylene blue-multiwalled carbon nanotubes. Electroanalysis 22:277–285
39. Arias P, Ferreyra NF, Rivas GA, Bollo SJ (2009) Glassy carbon electrodes modified with CNT dispersed in chitosan: analytical applications for sensing DNA–methylene blue interaction. J Electroanal Chem 634:123–126
40. Yan Y, Zhang M, Gong K, Su L, Guo Z, Mao L (2005) Adsorption of methylene blue dye onto carbon nanotubes: a route to an electrochemically functional nanostructure and its layer-by-layer assembled nanocomposite. Chem Mater 17:3457–3463
41. Zhang D, Fu L, Liao L, Dai B, Zou R, Zhang C (2012) Electrochemically functional graphene nanostructure and layer-by-layer nanocomposite incorporating adsorption of electroactive methylene blue. Electrochim Acta 7:71–79
42. Pakapongpan S, Palangsuntikul R, Surareungchai W (2011) Electrochemical sensors for hemoglobin and myoglobin detection based on methylene blue-multiwalled carbon nanotubes nanohybrid-modified glassy carbon electrode. Electrochim Acta 56:6831–6836
43. Liu H, Gao J, Xue M, Zhu N, Zhang M, Cao T (2009) Processing of graphene for electrochemical application: noncovalently functionalize graphene sheets with water-soluble electroactive methylene green. Langmuir 25:12006–12010
44. Liu Q, Li Y, Zhang L, Li D, Fan C, Long Y (2010) Comparative studies on electrocatalytic activities of chemically reduced graphene oxide and electrochemically reduced graphene oxide noncovalently functionalized with poly(methylene blue). Electroanalysis 22:2862–2870
45. Sylvestre JP, Poulin S, Kabashin AV, Sacher E, Meunier M, Luong JHT (2004) Surface chemistry of gold nanoparticles produced by laser ablation in aqueous media. J Phys Chem B 108:16864–16869
46. Gurunathan S, Han JW, Eppakayala V, Kim JH (2013) Biocompatibility of microbially reduced graphene oxide in primary mouse embryonic fibroblast cells. Colloids Surf B 105:58–66
47. Zou F, Yu Y, Cao N, Wu L, Zhi J (2011) A novel approach for synthesis of TiO2–graphene nanocomposites and their photoelectrical properties. Scr Mater 64:621–624
48. Wang Z, Shang K, Dong J, Cheng Z, Ai S (2012) Electrochemical immunoassay for subgroup of avian leukosis viruses using a glassy carbon electrode modified with a film of poly (3-thiophene boronic acid), gold nanoparticles, graphene and immobilized antibody. Microchim Acta 179:227–234

49. Liu Y, Liu L, Yuan M, Guo R (2013) Preparation and characterization of casein-stabilized gold nanoparticles for catalytic applications. Colloids Surf A 417:18–25
50. Sun C, Lee HH, Yang J, Wu C (2011) The simultaneous electrochemical detection of ascorbic acid, dopamine, and uric acid using graphene/size-selected Pt nanocomposites. Biosens Bioelectron 26:3450–3455
51. Wu G, Wu Y, Liu X, Rong M, Chen XM, Chen X (2012) An electrochemical ascorbic acid sensor based on palladium nanoparticles supported on graphene oxide. Anal Chim Acta 745:33–37
52. Shalini J, Sankaran KJ, Dong CL, Lee CY, Tai NW, Lin IN (2013) In situ detection of dopamine using nitrogen incorporated diamond nanowire electrode. Nanoscale 5:1159–1167
53. Yang A, Xue Y, Zhang Y, Zhang X, Zhao H, Li X, He Y, Yuan Z (2013) A simple one-pot synthesis of graphene nanosheet/SnO2 nanoparticle hybrid nanocomposites and their application for selective and sensitive electrochemical detection of dopamine. J Mater Chem B 1:1804–1811
54. Liu G, Li J, Wang L, Zong N, Yu S, Li F (2012) Discrimination of dopamine from ascorbic acid and uric acid on thioglycolic acid modified gold electrode. Anal Methods 4:609–611
55. Zhang Y, Pan Y, Su S, Zhang L, Li S, Shao M (2007) A novel functionalized single-wall carbon nanotube modified electrode and its application in determination of dopamine and uric acid in the presence of high concentrations of ascorbic acid. Electroanalysis 19:1695–1701
56. Dursun Z, Gelmez B (2010) Simultaneous determination of ascorbic acid, dopamine and uric acid at Pt nanoparticles decorated multiwall carbon nanotubes modified GCE. Electroanalysis 22:1106–1114
57. Cui R, Wang X, Zhang G, Wang C (2012) Simultaneous determination of dopamine, ascorbic acid, and uric acid using helical carbon nanotubes modified electrode. Sens Actuators B 161:1139–1143